



# Laboratory investigation of the mechanical properties of coal-rock combined body

Zhan-bo Cheng<sup>1,2,3</sup> · Liang-Hui Li<sup>1,2</sup> · Ya-Ning Zhang<sup>1,2,4</sup>

Received: 24 November 2018 / Accepted: 7 September 2019 / Published online: 26 November 2019  
© Springer-Verlag GmbH Germany, part of Springer Nature 2019

## Abstract

Understanding the behavior of the top-coal caving mining face and immediate roof can be used to enhance buffering effects. The mechanical properties of the coal-rock combined body (CRCB) play a vital role in the performance of overburden load transmittance and support resistance design. We define and derive the relative physical and mechanical parameters of CRCB to illustrate and analyze the influence of coal-rock height ratio (CRHR), coal and rock mass behavior, and interface parameters on CRCB mechanical properties. We conducted uniaxial compression tests to obtain uniaxial compressive strength (UCS), elastic modulus (EM), and the full range of stress–strain curves. Our results show that UCS is positively correlated with EM. However, CRCB EM and UCS decrease with increasing CRHR or effective coal-rock height ratio (ECRHR) and the slope of the curves gradually decreases. CRCB mechanical parameters increase linearly with EM of the coal or rock mass. Although increased coal-rock interface angles (IA) lead to increased CRCB mechanical parameters, the incremental value can be ignored. Sensitive analysis shows that the rank of influential factors on CRCB properties is CRHR/ECRHR > coal strength > rock strength > IA.

**Keywords** Coal-rock combined body · Mechanical parameters · Uniaxial compressive test · Influence factors

## Abbreviation

AE	acoustic emission	EM	elastic modulus
CCR	coal-cement ratio	FCR	fine soil-cement ratio
CRCB	coal-rock combined body	IA	interface angle
CRHR	coal-rock height ratio	RS	rock strength
CS	coal strength	TCCM	top-coal caving mining
ECRHR	effective coal-rock height ratio	UCS	uniaxial compressive strength

✉ Zhan-bo Cheng  
Z.Cheng.4@warwick.ac.uk

Liang-Hui Li  
lilianghui@cumt.cn

Ya-Ning Zhang  
zynmining@163.com

<sup>1</sup> School of Energy and Mining Engineering, China University of Mining and Technology–Beijing, Beijing 100083, China

<sup>2</sup> Coal Industry Engineering Research Center of Top-coal Caving Mining, Beijing 100083, China

<sup>3</sup> School of Engineering, University of Warwick, CV47AL, Coventry, UK

<sup>4</sup> Research Institute of Coal Strategy and Planning, Coal Industry Planning Institute, Beijing 100120, China

## Introduction

The reserves, production, and consumption of energy are global concerns (Dudley 2018) (Fig. 1). China is the largest coal producer and consumer with roughly 45% of global exploration and thick coal seam production (Qian et al. 2018; Wang 2018). Thick coal seams therefore play a vital role in providing the world's annual coal supplies. Top-coal caving mining (TCCM) presents a range of advantages compared with slice mining and large cutting height mining. For example, TCCM greatly reduces the labor intensity and material consumption in the workplace, which substantially reduces overhead costs. TCCM is also feasibly applied in complex geological conditions, particularly in steeply-inclined and thick coal seams. TCCM is therefore the dominant thick coal seam mining method because of its technical and economic advantages (Wang 2009; Meng et al. 2014).

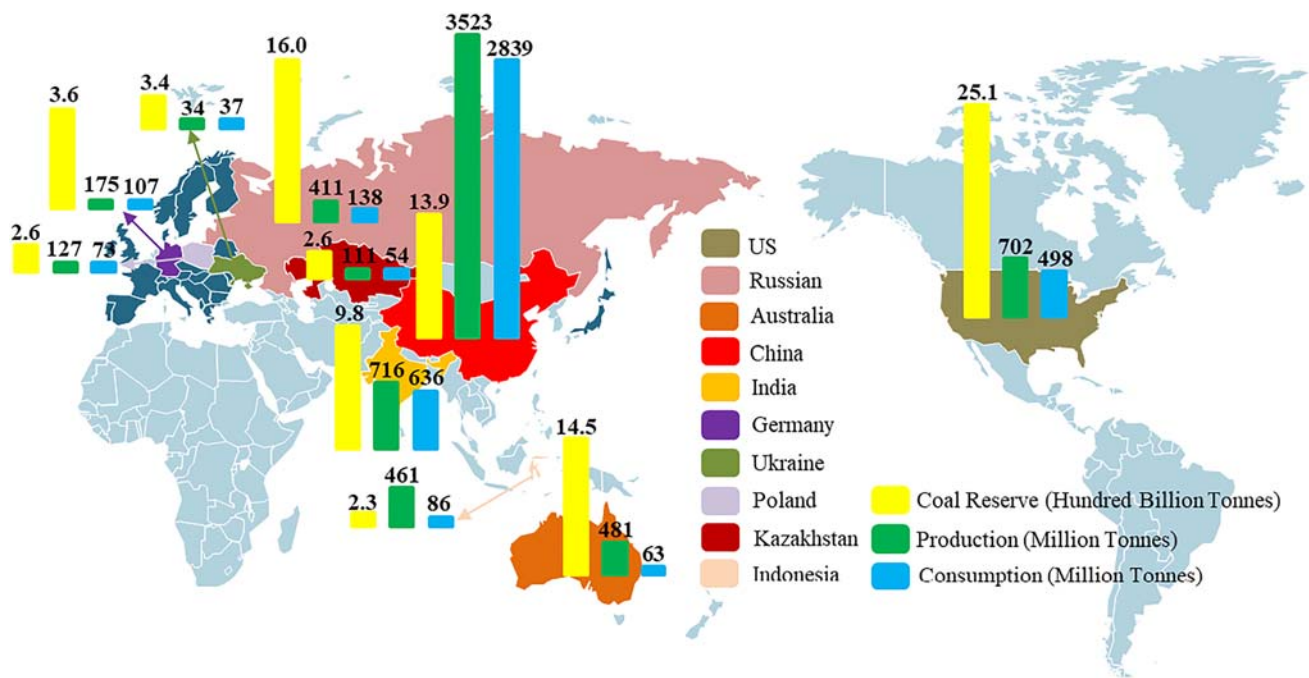


**Fig. 1** The coal reserves, production, and consumption of main countries

The top coal and immediate roof form a specific composite structure in the TCCM face. The feature serves as a cushion layer that undertakes and transfers overburden loads onto support equipment. The deformation resistance ability of the cushion layer is therefore critical for evaluating the resistance support design. Reasonable selection of the support type plays a fundamental role in the assortment of three machines in the working face. The excavation of underground openings leads to the formation of disturbed and damaged zones (Tsang et al. 2005; Wang et al. 2017a; Masri et al. 2014; Kong et al. 2019; Liu and Cheng 2019; Sun et al. 2019). Resistance support determination is used to control the surrounding rock and is extremely important for guaranteeing safe and efficient mining. Characterization and analyses of the cushion layer, in addition to pure coal or rock mass, is therefore necessary for appropriate support determination in the TCCM face (Hao et al. 2009; Li et al. 2002; Kirzhner and Rozenbaum 2001; Ruppel and Langosch 2006; Zhang et al. 2019; Xinjie et al. 2019).

The stability determination of a two-body system composed of a roof, floor, and coal was first proposed by Petukhov and Linkov (1979). In recent years, many scholars have reported the burst potential and energy dissipation of the coal-rock combined body (CRCB) using acoustic emission (AE), infrared thermal imaging, and other methods, and a series of beneficial results were obtained (Wu and Wang 1998; Zhao et al. 2015; Xue et al. 2012; Tan et al. 2016; Zhao et al. 2008; Jiang et al. 2007; Li et al. 2012; Liu et al. 2004; Zhang et al. 2012; Yang et al. 2017; Zhao et al. 2014; Lv et al. 2019; Liu et al. 2018a). Wang et al. (2014) performed a double-shear frictional test under biaxial loading and illustrated the space-time evolution of the displacement field as well as AE characteristics during sliding. Coal has

been shown to mainly govern the mechanical properties and deformation failure characteristics of CRCB, and cracks occurring in the coal reduce the CRCB uniaxial compression strength (Chen et al. 2018). The results of experimental tests, theoretical analyses and numerical simulations have shown that the UCS and EM of CRCB significantly increase with decreasing CRHR and increasing confining pressure and rock strength (Wang et al. 2017b; Liu et al. 2018b; Tan et al. 2018; Cheng et al. 2019a; Cheng et al. 2019b). The rock strain recovery introduces a loading effect on the failure of coal after CRCB failure. The incident and reflective energy of coal-rock samples also sharply increases with loading rate, while the transmitted energy remains largely unaffected. The entire CRCB dynamic stress–strain curve shows a double-peak feature under high loading rates, which can be divided into four stages (Gong et al. 2018). Wang and Tian (2018) used numerical simulations to explore the mechanical properties, crack evolution characteristics, and propagation forms of the initial and final crack distribution of coal-rock specimens with different fracture holes. They concluded that fracture angle significantly influences CRCB mechanical behavior. Although previous studies have addressed many aspects of CRCB behavior, the failure mechanism and mechanical behavior remains poorly understood.

In this study, we deepen the fundamental understanding of CRCB mechanical behavior and provide a theoretical foundation for determining support resistance in the TCCM face. We consider the influence of coal-rock height ratio (CRHR), coal strength (CS), rock strength (RS), coal-rock interface angle (IA), and effective coal-rock height ratio (ECRHR). Uniaxial compressive tests were conducted to obtain the uniaxial compressive strength (UCS), elastic modulus (EM), and full range of CRCB stress–strain curves.



(a) Moulds



(b) Partial samples

Fig. 2 Moulds and samples

## Experimental procedure

### Sample preparation

The mechanical behavior of coal and rock masses was simulated by adopting coal and fine soil mixed with different cement contents. The strength of each material generally increases with cement content. The specimens were synthesized to match engineering scenarios of coal and rock masses in a typical TCCM face.



Fig. 3 Overall WAM-600B system

Table 1 Key parameters of WAM-600B

Parameter	Value
Displacement range	150 mm
Displacement accuracy	±1%
Displacement resolution	0.001 mm
Axial force accuracy	±1%

Standard cubic 10 × 10 × 10 cm CRCB specimens were prepared from coal and rock masses with different CRHR. We used a coal-rock combination pattern with coal on the bottom according to TCCM face conditions in the field. Although cylindrical samples exhibit different failure patterns and failure strength levels, we chose cubic samples in this study because they are easier to prepare and test (Viso et al. 2008; Chang et al. 2015) and they meet the requirements for determining CRCB physical and mechanical parameters. Sketches of the molds and partial specimens are shown in Fig. 2.

We employed a standard sample preparation procedure to ensure consistent sample quality. The inside of the cubic molds was first treated with grease to reduce demolding friction. The mixed coal powder with different cement contents and a suitable moisture content of 30% (ratio of water mass to all solid mass) was then placed in the cubic molds. A piece of iron was used to form uniform layers until reaching the setting height. The same approach was used for the rock mass using fine soil mixed with different cement contents and 30% suitable moisture content. To minimize contamination, the surface of the uppermost coal mass layer was scraped to a depth of about 1 cm before inserting the rock mass to ensure direct contact between the rock and coal without the use of adhesives at the interface. The top of the specimens was then covered with plastic film to prevent water loss. The molds were dismantled after 24 h and specimens were kept at room temperature for 7 days without the plastic film. The mass of each specimen was measured to obtain the density prior to testing.

Table 2 Details for analyzing coal-rock height ratio (CRHR)

CRHR	CCR	FCR	Density (g/cm <sup>3</sup> )
Pure rock mass	1:1	1:1.5	1.96
2:8			1.85
4:6			1.73
5:5			1.68
6:4			1.62
7:3			1.56
8:2			1.50
Pure coal mass			1.39

**Table 3** Pure coal and rock mass conditions

Material	The ratio of material to cement	Density (g/cm <sup>3</sup> )
Coal	2:1	1.18
	1:1	1.39
	1:1.5	1.51
	1:2	1.59
Fine soil	1:0.8	1.87
	1:1.2	1.93
	1:1.5	1.96
	1:2	2.05

### Test apparatus

Samples were measured using a WAW-600B computerized electro-hydraulic servo-controlled universal testing machine (Fig. 3). The apparatus consisted of a 600-kN axial actuator, axial load and displacement transducers, screen display, and results treatment scheme. The key parameters of the apparatus are listed in Table 1.

### Testing schemes

Uniaxial compressive tests were performed with a strain-controlled loading rate of 0.5 mm/min. The comprehensive mechanical behavior of CRCB was evaluated considering the influence of CRHR, CS, RS, and coal-rock interface properties IA and ECRHR. Pure coal and rock masses were also tested with variable cement content to obtain mechanical parameters of the pure materials. Three specimens were tested under each condition and the average of each series was adopted to improve the accuracy and reproducibility of all tests. The testing conditions are listed in Tables 2, 3, 4, and 5.

**Table 4** Details for analyzing coal strength (CS) and rock strength (RS)

CRHR	Coal strength		Density (g/cm <sup>3</sup> )	Rock strength		Density (g/cm <sup>3</sup> )
	CCR	FCR		FCR	CCR	
4:6	2:1	1:1.5	1.65	1:0.8	1:1	1.69
	1:1		1.73	1:1.5		1.73
	1:2		1.81	1:2		1.79
5:5	2:1		1.57	1:0.8		1.63
	1:1		1.68	1:1.5		1.68
	1:2		1.78	1:2		1.72
8:2	2:1		1.34	1:0.8		1.49
	1:1		1.50	1:1.5		1.50
	1:2		1.66	1:2		1.52

**Table 5** Details for analyzing coal-rock interface properties

$\alpha$	ECRHR	CCR	FCR	Density (g/cm <sup>3</sup> )
(a) Effective coal-rock height ratio (ECRHR)				
0°	1:2	1:1	1:1.5	1.77
	1:1			1.68
	2:1			1.58
15°	1:2			1.72
	1:1			1.68
	2:1			1.63
(b) Interface angle (IA)				
0°	1:1	1:1	1:1.5	1.68
10°				1.68
15°				1.68

### Theoretical solution of mechanical properties

In this section, we demonstrate the theoretical solution of some mechanical and physical parameters. The UCS is calculated as:

$$R = \frac{P}{A} \quad (1)$$

$$A = l^2 \quad (2)$$

where  $R$ ,  $P$ ,  $A$ , and  $l$  are UCS, the maximum failure uniaxial loading, specimen surface area, and specimen size, respectively.

CRCB exhibits a deformation-dependent behavior, similar to most geomaterials. A typical CRCB stress–strain curve is shown in Fig. 4. The process can be divided into six stages: compaction, linear elastic deformation, inelastic deformation, strain-hardening, post-peak softening, and residual strength. The linear elastic deformation stage dominates the linear portions of the stress–strain curves and matrix deformation. The material exhibits intact geomaterial behavior characterized by

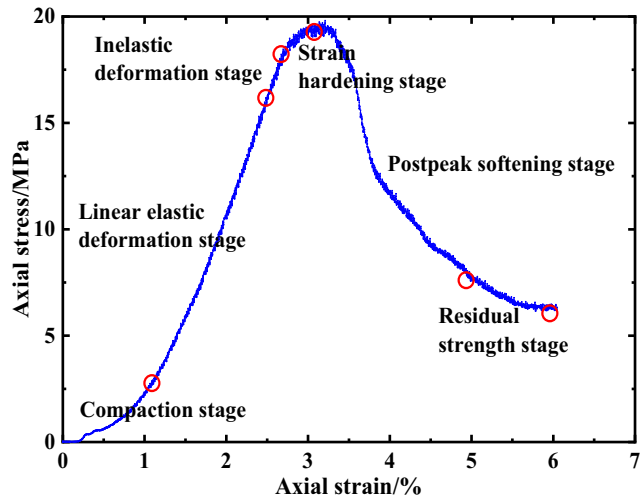


Fig. 4 Typical stress–strain curve of a coal-rock combined body (CRCB)

constant stiffness during this stage. The EM can be expressed as:

$$E = \frac{\Delta\sigma}{\Delta\varepsilon} \tag{3}$$

where  $E$ ,  $\Delta\sigma$ , and  $\Delta\varepsilon$  are EM, and stress and strain increments, respectively.

In the occurrence of IA, the coal to rock height ratio in CRCB is not effectively represented by a single side length. It is therefore necessary to define an effective coal to rock height ratio. A specimen schematic is shown in Fig. 5. The effective height of a single material is represented by the ratio of the cross-section of the single material parallel to the axial-force direction of the entire CRCH length. Thus, ECRHR is defined as the ratio of the effective coal height to that of rock.

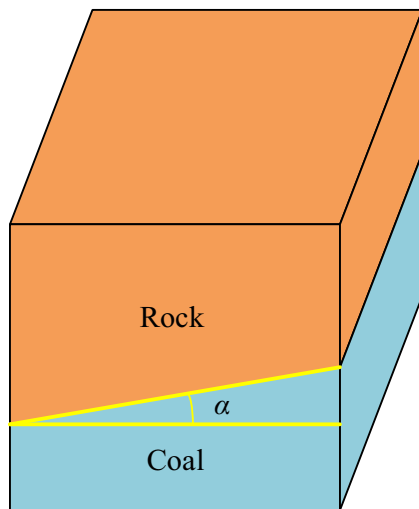


Fig. 5 Coal-rock combined body (CRCB) with the occurrence of an interface angle (IA)

Separate coal and rock coordinates in CRCB are established, as shown in Fig. 6.

The equations of an interface line can be expressed as follows from different perspectives.

$$y = x \tan\alpha + L_1 - L \tan\alpha \tag{4}$$

$$y = -x \tan\alpha + L_2 \tag{5}$$

The expressions of effective height of each material are shown in Eqs. (6) and (7), respectively.

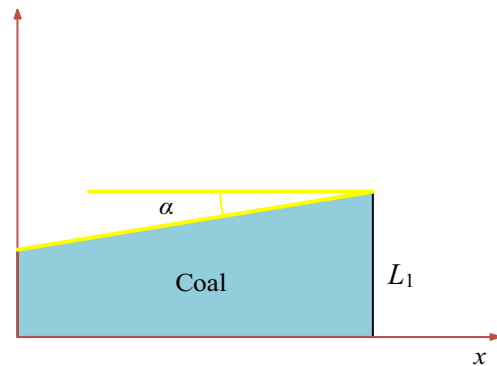
$$l_c = \frac{\int_0^L (x \tan\alpha + L_1 - L \tan\alpha) dx}{L} = L_1 - \frac{1}{2} L \tan\alpha \tag{6}$$

where  $l_c$  is the effective coal height.

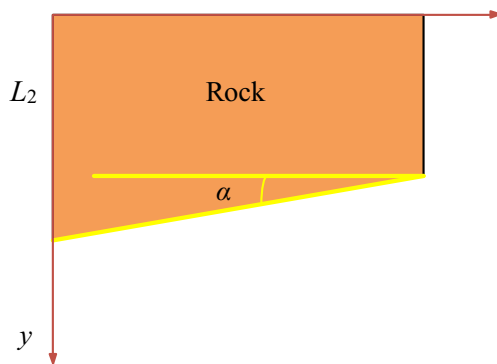
$$l_r = \frac{\int_0^L (-x \tan\alpha + L_2) dx}{L} = L_2 - \frac{1}{2} L \tan\alpha \tag{7}$$

where  $l_r$  is the effective rock height. The ECRHR is expressed as:

$$r' = \frac{l_c}{l_r} \tag{8}$$



(a) Coal



(b) Rock

Fig. 6 Coordinate sketch map

Cheng et al. (2018) proposed a theoretical solution of EM of CRCB with or without IA:

$$E = \frac{k'}{A} = \frac{E_1 E_2 (r + 1)^2}{E_1 + E_2 r^2 + 2r \sqrt{E_1 E_2}} \quad (9)$$

where  $k'$  is pull-pressing rigidity,  $E_1$  and  $E_2$  are the EMs of the coal and rock masses, respectively, and  $r$  is the CRHR in the case of no contact angle in the CRCB. If a contact angle occurs,  $r$  can be used as:

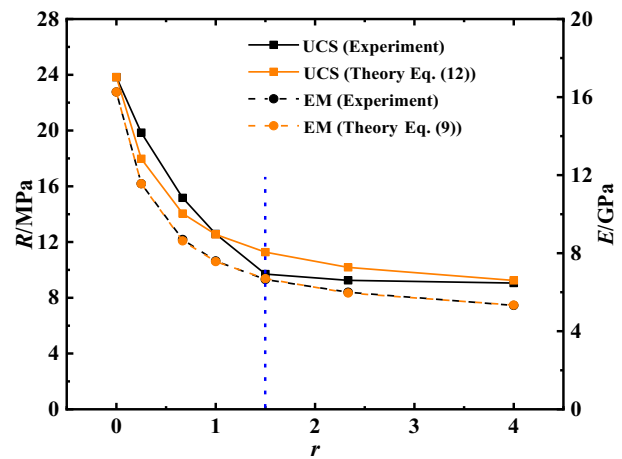
$$r = \frac{r'l - \frac{1}{2} \frac{r'l + 1}{1 + \tan\alpha} \tan\alpha}{1 - \frac{1}{2} \frac{r'l + 1}{1 + \tan\alpha} \tan\alpha} \quad (10)$$

$$r'l = \frac{L_1}{L_2} \quad (11)$$

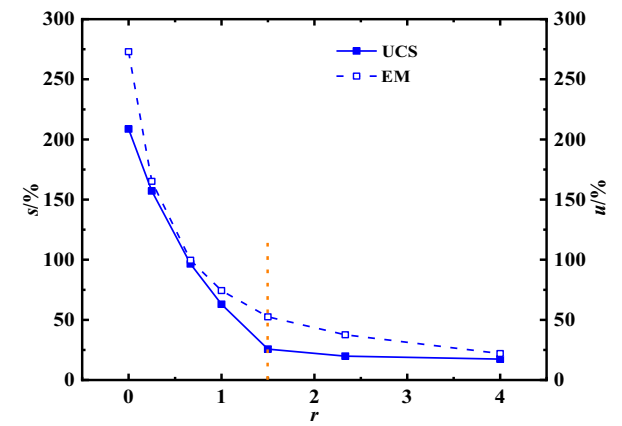
## Results and discussion

### Coal-rock height ratio

The overall failure forms and stress–strain curves of specimens with different CRHR are shown in Fig. 7. The peak axial stress occurs in the range from 2% to 3.5%. Serious failure occurred in the coal mass, and coal spalling was observed. Figure 8 illustrates the curves of UCS and EM versus



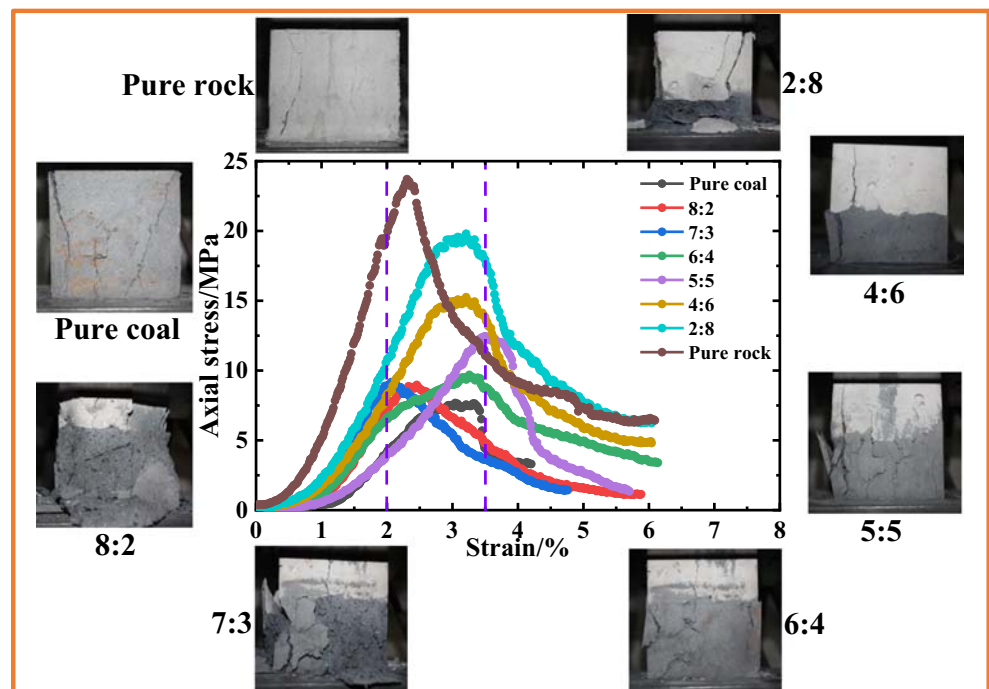
(a) UCS and EM versus CRHR



(b) Increment ratio versus CRHR

Fig. 8 Influence of the coal-rock height ratio (CRHR) on the mechanical parameters of coal-rock combined body (CRCB)

Fig. 7 Typical stress–strain curves and failure forms with different coal-rock height ratios (CRHR)



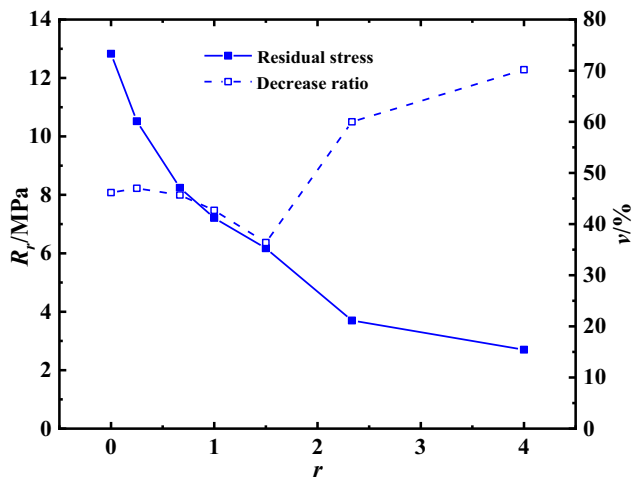


Fig. 9 Influence of the coal-rock height ratio (CRHR) on the coal-rock combined body (CRCB) in the residual stage

CRHR using the same properties of the coal and rock masses. Pure coal results are not shown in Fig. 8 because their CRHR is essentially infinite. Sample preparation in a 10-cm-high mold restricts the CRHR range to 0–4 (e.g., a CRHR of 4 is obtained when the coal mass height is 8 cm). Nevertheless, the CRHR range adopted in this study is consistent with most engineering applications.

The CRCB mechanical parameters decrease with increasing CRHR when the EM of pure coal and rock are 4 and 16 GPa, respectively, and the corresponding UCS are 8 and 24 MPa, respectively (Fig. 8a). Two critical CRHR values are observed. When CRHR = 1.5, the negative slope decreases and when CRHR = 3, the CRCB mechanical parameters remain essentially constant (Fig. 8). The CRCB UCS is strongly

and positively related with EM. The theoretical expression for UCS can therefore be obtained as:

$$R = \frac{R_1 R_2 (r + 1)^2}{R_1 + R_2 r^2 + 2r \sqrt{R_1 R_2}} \quad (12)$$

where  $R_1$  and  $R_2$  are the UCS of the coal and rock mass, respectively. The experimental results and theoretical calculations of the UCS and EM of CRCB are in generally good agreement. Equation (12) can therefore be considered reasonable for estimating the UCS of CRCB.

To more clearly illustrate the influence of CRHR on CRCB mechanics parameters, we define two values to represent the incremental values of UCS and EM under different CRHR:

$$s = [(R - R_1) / R_1] \times 100\% \quad (13)$$

$$u = [(E - E_1) / E_1] \times 100\% \quad (14)$$

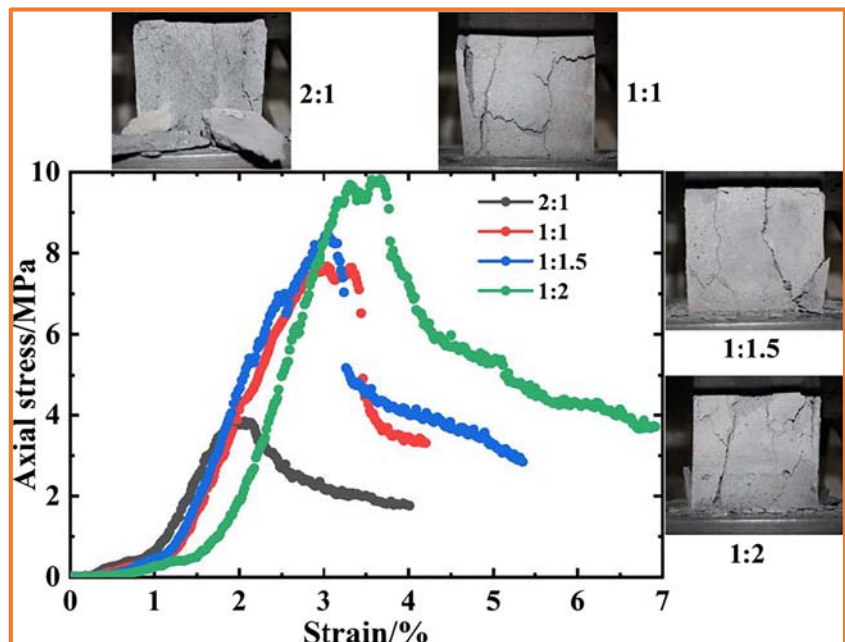
where  $s$  and  $u$  are the increment ratios of UCS and EM of CRCB compared with those of pure coal, respectively. Both values are shown in Fig. 8b as a function of CRHR. The results indicate that CRHR has little influence on the CRCB mechanical properties until the proportion of coal body reaches a certain value.

The CRCB residual stress and its decrease ratio compared with peak UCS are shown in Fig. 9. The decrease ratio can be expressed as follows:

$$v = [(R_p - R_r) / R_p] \times 100\% \quad (15)$$

where  $R_p$  and  $R_r$  are the peak and residual CRCB uniaxial compressive strength, respectively.

Fig. 10 Stress–strain curves and failure forms of coal samples



The residual axial stress decreases with increasing CRHR at a gradually decreasing rate. The decrease ratio reduces to a minimum at CRHR = 1.5 and then increases. The loss percent in the residual stage tends to remain roughly 45% for CRHR less than 1.

**Coal strength**

Cement has been shown in previous studies to provide sufficient additional strength for weakened materials. The cement content therefore significantly influences the coal and rock mechanical parameters during sample preparation. The full range of stress–strain curves and failure types of the four different coal-cement ratios (CCR) are shown in Fig. 10.

The UCS and EM of pure coal increases with cement content and the corresponding increment ratio decreases. The basic mechanical parameters of pure coal are similar to runs with CCR of 1:1 and 1:1.5, as shown in Fig. 11. We select three coal mass categories (CCR = 2:1, 1:1, 1:2) to demonstrate the influence of CS on CRCB under three different CRHR situations. The corresponding UCSs of pure coal with different CCR are 4, 8, and 10 MPa, respectively, and the EMs of pure rock are 2, 4, and 6 GPa, respectively. The UCS and EM of the rock mass remain constant at 24 MPa and 16 GPa, respectively.

The CRCB mechanical parameters increase with CS and show good agreement between the experiments and calculations (Fig. 12). The UCS and EM of CRCB increase linearly with increasing coal UCS and EM. The incremental slope of UCS is similar to that of EM, and increasing CS is observed to significantly influence the combined body. For example, when the UCS of the coal samples increases from 4 to 10 MPa, the CRCB UCS increases in each of the three CRHR conditions, from 10 to 19 MPa, 8 to 15 MPa, and 5 to 12 MPa.

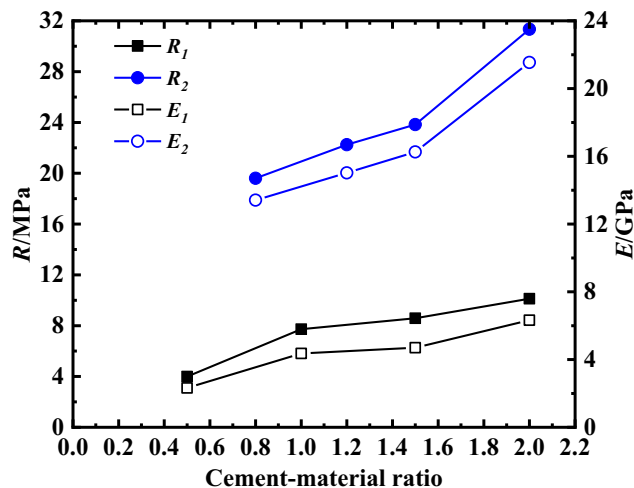
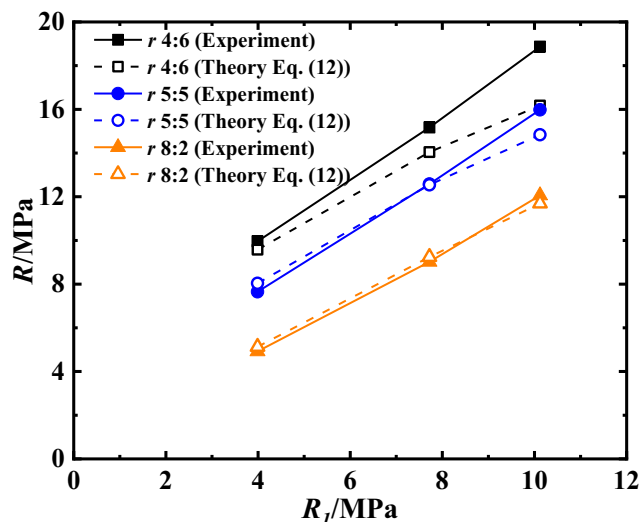
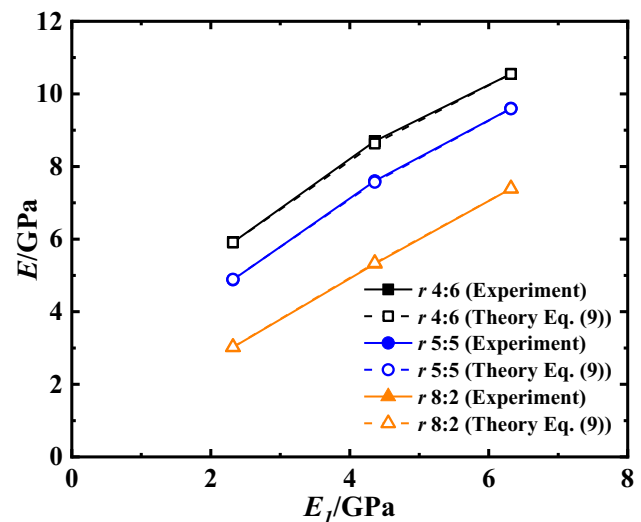


Fig. 11 Uniaxial compressive strength (UCS) and elastic modulus (EM) of coal and rock masses as a function of cement-material ratio



(a) UCS



(b) EM

Fig. 12 Influence of coal strength (CS) on the mechanical parameters of the coal-rock combined body (CRCB)

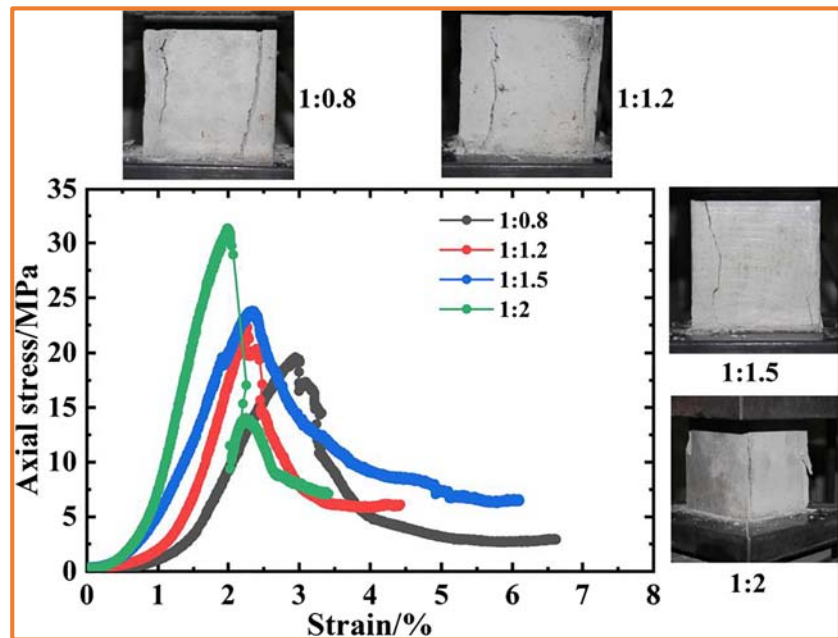
**Rock strength**

To assess the influence of RS on CRCB, we prepared and performed uniaxial loading tests on samples with four different fine soil-cement ratios (FCR). The full range of stress–strain curves and failure forms are shown in Fig. 13.

From Eqs. (9) and (14), the UCS and EM of rock mass are shown to increase with cement content, as shown in Fig. 11. No difference is observed for samples with FCR between 1:1.2 and 1:1.5. We therefore adopt three rock mass types with FCR = 1:0.8, 1:1.2, and 1:2 to efficiently and accurately compare the effects of RS on the mechanical properties of CRCB. The corresponding UCS values increase from 20 to 22 to 31 MPa, and the EM increases from 13 to 15 to 22 GPa. The UCS and EM of the coal mass remain constant at



**Fig. 13** Stress–strain curves and failure forms of rock specimens



8 MPa and 4 GPa, respectively. The CRCB uniaxial compression results with different CRHR are shown in Fig. 14. The experimental results match well with the theoretical analysis.

The UCS and EM of CRCB increase linearly with increasing rock UCS and EM. The incremental UCS slope is also similar to that of EM. All CRCB mechanical parameters are smaller than those of the pure rock mass. However, RS shows a range of effects on CRCB under different CRHR. Specifically, RS affects CRCB progressively less with increasing CRHR. For example, when CRCR = 8:2, the CRCB UCS increases only from 8 to 9 MPa, whereas the rock UCS increases from 20 to 31 MPa. The mechanical properties of CRCB change marginally with increasing RS when the CRHR is greater than approximately 5:5, and the sensitivity of RS influence on CRCB is smaller than that of CS.

### Coal-rock interface properties

We consider two factors involving IA and ECRHR to determine the influence of the coal-rock contact surface on CRCB mechanical properties. Two kinds of preparation schemes were designed separately with variable IA and ECRHR. The CCR and FCR were selected as 1:1 and 1:1.5, respectively, and laboratory tests were conducted to study the effects of contact properties on the mechanical properties of the composite material.

### Effective coal-rock height ratio

As previously mentioned, the ECRHR is defined when IA occurs. To analyze the effect of ECRHR on CRCB mechanical parameters, we select three ECRHR values (1:2, 1:1, 2:1)

under two IA situations. The theoretical solution of UCS and EM is obtained from Eqs. (9)–(12). Figure 15 illustrates the experimental and theoretical results of CRCB with increasing ECRHR.

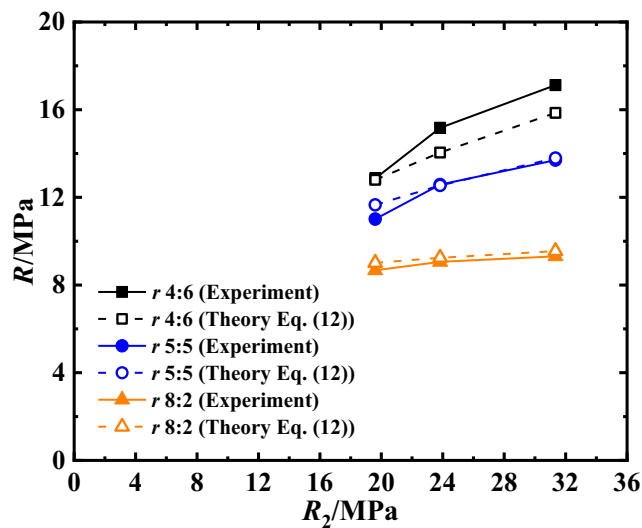
The ECRHR is equal to CRHR if the coal-rock contact surface is horizontal and substantially better agreement is obtained between the experiments and calculations (Fig. 15). Overall, the mechanical properties of CRCB decrease with increasing ECRHR with a gradually decreasing trend. For example, for samples with IA = 15°, the CRCB EM decreases from 10 to 8 GPa when the ECRHR increases from 0.5 to 1, and then to 6 GPa when the ECRHR = 2. The same behavior is observed for samples with different IA.

### Interface angle

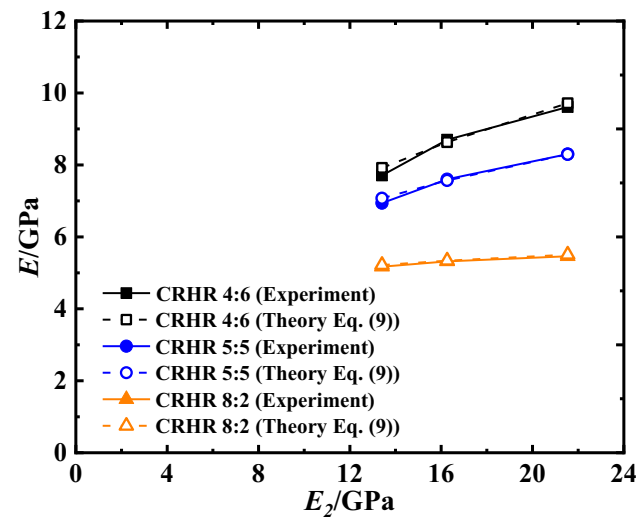
We select samples with three IAs (0°, 10°, 15°) and ECRHR = 1 to assess the effect of IA on CRCB mechanical parameters. The CRCB UCS increases linearly from 12 to 13 MPa with increasing IA, and the CRCB EM increases from 7 to 8 GPa (Fig. 16). Good agreement is observed between the experimental and theoretical results. However, the influence of IA on CRCB mechanical parameters is only marginal, which is consistent with the results of Li et al. (2012).

### Limitations and future work

The results obtained in this study show that the mechanical properties of CRCB are affected by several factors, including CRHR/ECRHR, CS, RS, and IA. Nevertheless, some



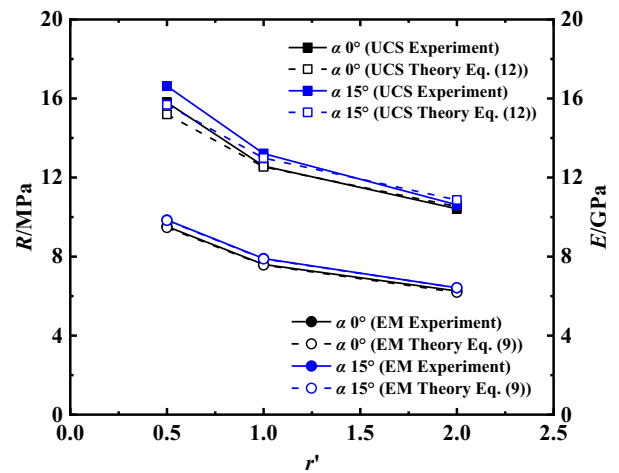
(a) UCS



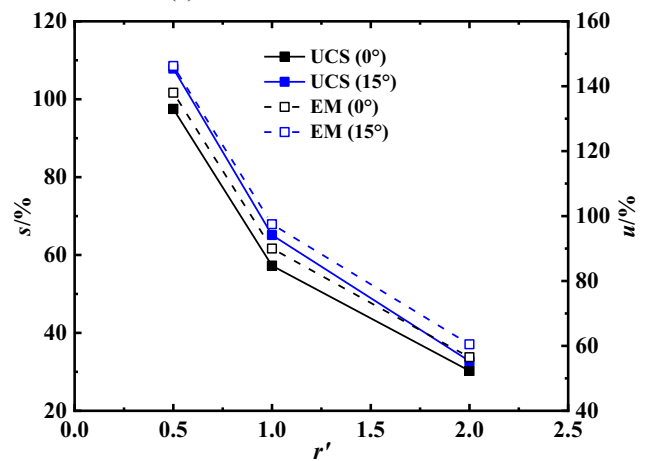
(b) EM

Fig. 14 Influence of rock strength (RS) on the mechanical parameters of coal-rock combined body (CRCB)

limitations are also encountered. First, the current study considers top coal and rock as complete materials, whereas gradual failure of these materials is known to occur owing to cyclic normal stress as well as continuous unloading of confining pressure during excavation. Additional attention is therefore required on the law of energy transfer and dissipation during the entire uniaxial compressive process and specimens should be prepared with joint cracks. The testing procedures can also be improved, particularly for situations of  $CS > RS$  and for mudstone. The CRCB mechanical parameter behavior under these conditions warrants further discussion. Variable IA and loading rate are also important to simulate CRCB in complex mining environments. The mechanical properties of CRCB can be combined with determination methods of support working resistance, which is



(a) UCS and EM versus ECRHR



(b) Increment ratio versus ECRHR

Fig. 15 Influence of the effective coal-rock height ratio (ECRHR) on the mechanical parameters of coal-rock combined body (CRCB)

fundamental for selecting the support type and controlling the stability of surrounding rock in the TCCM face, and will be addressed in future studies.

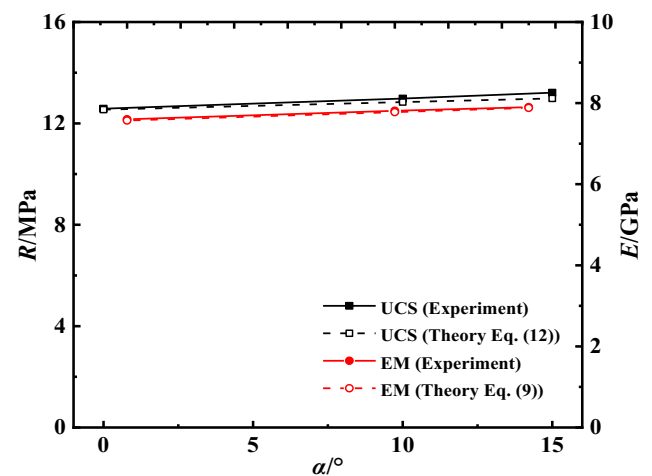


Fig. 16 Uniaxial compressive strength (UCS) and elastic modulus (EM) as a function of interface angle (IA)

## Conclusions

We performed extensive experimental investigations to evaluate the mechanical behavior of CRCB under uniaxial compression. The experiments involved CRHR (pure coal mass, 8:2, 7:3, 6:4, 5:5, 4:6, 2:8, pure rock mass), S with different CCR (2:1, 1:1, 1:2), RS with different FCR (1:0.8, 1:1.5, 1:2), ECRHR (2:1, 1:1, 1:2), and IA (0°, 10°, 15°). The following conclusions may be drawn from the present study.

The CRCB UCS is strongly and positively related with EM, and theoretical determination of UCS can be obtained via analogy. The results demonstrate good agreement between experiments and calculations in terms of the CRCB UCS and EM for all samples. Tensile failure is observed in the CRCB specimens.

The mechanical parameters of CRCB decrease with increasing CRHR. A dramatic change is observed for CRHR less than 1.5, whereas the mechanical behavior remains essentially unchanged after reaching CRHR >3. Compared with peak UCS, the decreasing ratio in the residual stage first decreases and then increases with CRHR. The lowest loss percent is obtained when CRHR = 1.5; however, the loss percent is roughly 45% if CRHR <1.

The influence of CS and RS on CRCB is similar. The CRCB UCS and EM increase linearly with increasing UCS and EM of pure coal or rock mass. However, the CRHR affects the influence of RS on CRCB. Greater CRHR reduces the effect of changing RS.

When IA occurs between the rock and coal parts in CRCB, the CRCB mechanical properties decrease with increasing ECRHR and the decreasing trend tends to slow. The UCS and EM of CRCB increase linearly with IA, although the influence is marginal. Sensitive analysis among all influential factors reveals the following ranking of factors that influence CRCB: CRHR/ECRHR > CS > RS > IA.

**Acknowledgements** The authors acknowledge support from the China Scholarship Council (CSC). Many thanks to Baojin Yan for technical guidance in the uniaxial compressive test procedure. We thank the editors and anonymous reviewers for their valuable time and suggestions.

## References

- Chang I, Im J, Prasadhi AK, Cho GC (2015) Effects of xanthan gum biopolymer on soil strengthening. *Constr Build Mater* 74:65–72. <https://doi.org/10.1016/j.conbuildmat.2014.10.026>
- Chen Y, Zuo J, Liu D, Wang Z (2018) Deformation failure characteristics of coal-rock combined body under uniaxial compression: experimental and numerical investigations. *Bull Eng Geol Environ* 78(5):3449–3464. <https://doi.org/10.1007/s10064-018-1336-0>
- Cheng Z, Pan W, Li X, Sun W (2019b) Numerical simulation on strata behaviours of TCCWF influenced by coal-rock combined body. *Geomechanics and Engineering* 19(3):269–282. <https://doi.org/10.12989/gae.2019.19.3.269>
- Cheng Z, Yang S, Li L, Zhang L (2019a) Support working resistance determined on top-coal caving face based on coal-rock combined body. *Geomechanics and Engineering* 19(3):255–268. <https://doi.org/10.12989/gae.2019.19.3.255>
- Cheng Z, Zhang Y, Li L, Lv H (2018) Theoretical solution and analysis of the elastic modulus and foundation coefficient of coal-rock combination material. *Int J Mater Sci Res* 1(1):23–31. <https://doi.org/10.18689/ijmsr-1000104>
- De-Zhong Kong, Zhan-Bo Cheng, Shang-Shang Zheng. (2019) Study on the failure mechanism and stability control measures in a large-cutting-height coal mining face with a deep-buried seam. *Bulletin of Engineering Geology and the Environment* 78 (8):6143–6157. <https://doi.org/10.1007/s10064-019-01523-0>
- Dudley B (2018) BP statistical review of world energy. <https://www.bp.com>
- Gong F, Ye H, Luo Y (2018) The effect of high loading rate on the behavior and mechanical properties of coal-rock combined body. *Shock Vib*. <https://doi.org/10.1155/2018/4374530>
- Hao X, Xu J, Zhu W, Wang X (2009) Determination of the reasonable support working resistance. *Procedia Earth Planet Sci* 1(1):1398–1405. <https://doi.org/10.1016/j.proeps.2009.09.216>
- Jiang Y, Zhao Y, He M, Peng S (2007) Investigation on mechanism of coal mine bumps based on mesoscopic experiments. *Chin J Rock Mech Eng* 26(5):901–907
- Kirzhner F, Rozenbaum M (2001) Behavior of the working fluid in mechanized support in permafrost. *J Cold Reg Eng* 15(3):170–185. [https://doi.org/10.1061/\(ASCE\)0887-381X\(2001\)15:3\(170\)](https://doi.org/10.1061/(ASCE)0887-381X(2001)15:3(170))
- Kong D-Z, Cheng Z-B, Zheng S-S (2019) Study on the failure mechanism and stability control measures in a large-cutting-height coal mining face with a deep-buried seam. *Bulletin of Engineering Geology and the Environment* 78(8):6143–6157. <https://doi.org/10.1007/s10064-019-01523-0>
- Li H, Zhou Y, Jian R (2002) The feature of support resistance in fully mechanized top-coal caving working face. *Proc Mining Sci Safety Technol* 3:134–140
- Li X, Kang L, Li H, Ouyang Z (2012) Three-dimensional numerical simulation of bust-prone experiments about coal-rock combination. *J China Coal Soc* 36(12):2064–2067
- Liu F, Guo ZR, Lv HY, Cheng ZB (2018a) Test and analysis of blast wave in mortar test block. *Int J Rock Mech Min Sci* 108:80–85. <https://doi.org/10.1016/j.ijrmm.2018.06.003>
- Liu J, Tang C, Zhu W, Yang T (2004) Rock-coal model for studying the rockburst. *Chin J Geotech Eng* 2:276–280
- Liu X-J, Cheng Z-B (2019) Changes in subsidence-field surface movement in shallow-seam coal mining. *Journal of the Southern African Institute of Mining and Metallurgy* 119(2). <https://doi.org/10.17159/2411-9717/2019/v119n2a12>
- Liu X, Tan Y, Ning J, Lu Y, Gu Q (2018b) Mechanical properties and damage constitutive model of coal in coal-rock combined body. *Int J Rock Mech Min Sci* 110:140–150. <https://doi.org/10.1016/j.ijrmm.2018.07.020>
- Lv HY, Tang YS, Zhang LF, Cheng ZB, Zhang YN (2019) Analysis for mechanical characteristics and failure models of coal specimens with non-penetrating single crack. *Geomech Eng* 17(4):355–365. <https://doi.org/10.12989/gae.2019.17.4.355>
- Masri M, Sibai M, Shao J, Mainguy M (2014) Experimental investigation of the effect of temperature on the mechanical behavior of Tournemire shale. *Int J Rock Mech Min Sci* 70:185–191. <https://doi.org/10.1016/j.ijrmm.2014.05.007>
- Meng X, Wu H, Wang G (2014) Development and method selection of thick coal seam mining technology in China. *Coal Eng* 46(10):43–47
- Petukhov IM, Linkov AM (1979) The theory of post-failure deformations and the problem of stability in rock mechanics. *Int J Rock Mech Mining Sci Geomech Ab* 16(2):57–76. [https://doi.org/10.1016/0148-9062\(79\)91444-X](https://doi.org/10.1016/0148-9062(79)91444-X)

- Qian M, Xu J, Wang J (2018) Further on the sustainable mining of coal. *J China Coal Soc* 43(1):1–13. <https://doi.org/10.13225/j.cnki.jccs.2017.4400>
- Ruppel U, Langosch U (2006) New method for dimensioning of shield support to improve longwall roof control. *J Mines Met Fuels* 54(8):179–184
- Sun W, Du H, Zhou F, Shao J (2019) Experimental study of crack propagation of rock-like specimens containing conjugate fractures. *Geomechanics and Engineering* 17(4):323–331. <https://doi.org/10.12989/gae.2019.17.4.323>
- Tan Y, Guo W, Gu Q, Zhao T, Yu F, Hu S, Yin Y (2016) Research on the rockburst tendency and AE characteristics of inhomogeneous coal-rock combination bodies. *Shock Vib* 2:1–11. <https://doi.org/10.1155/2016/9271434>
- Tan Y, Liu X, Shen B, Ning J, Gu Q (2018) New approaches to testing and evaluating the impact capability of coal seam with hard roof and/or floor in coal mines. *Geomech Eng* 4(14):367–376. <https://doi.org/10.12989/gae.2018.14.4.367>
- Tsang CF, Bemier F, Davies C (2005) Geohydromechanical processes in the excavation damaged zone in crystalline rock, rock salt, and indurated and plastic clays-in the context of radioactive waste disposal. *Int J Rock Mech Min Sci* 42(1):109–125. <https://doi.org/10.1016/j.ijrmms.2004.08.003>
- Viso JRD, Carmona JR, Ruiz G (2008) Shape and size effects on the compressive strength of high-strength concrete. *Cem Concr Res* 38(3):386–395. <https://doi.org/10.1016/j.cemconres.2007.09.020>
- Wang G, Wu M, Wang R, Xu H, Song X (2017b) Height of the mining-induced fractured zone above a coal face. *Eng Geol* 216:140–152. <https://doi.org/10.1016/j.enggeo.2016.11.024>
- Wang J (2009) Theory and technology of thick seam mining. Metallurgical Industry Press, China
- Wang J (2018) Engineering practice and theoretical progress of top-coal caving mining technology in China. *J China Coal Soc* 43(1):43–51. <https://doi.org/10.13225/j.cnki.jccs.2017.4101>
- Wang K, Du F, Zhang X, Wang L, Xin C (2017a) Mechanical properties and permeability evolution in gas-bearing coal-rock combination body under triaxial. *Environ Earth Sci* 76(24):815. <https://doi.org/10.1007/s12665-017-7162-z>
- Wang T, Zhan S, Wang C (2014) Frictional sliding tests on combined coal-rock samples. *J Rock Mech Geotech Eng* 6(3):280–286. <https://doi.org/10.1016/j.jrmge.2014.03.007>
- Wang X, Tian L (2018) Mechanical and crack evolution characteristics of coal-rock under different fracture-hole conditions: a numerical study based on particle flow code. *Environ Earth Sci* 77(8):297. <https://doi.org/10.1007/s12665-018-7486-3>
- Wu L, Wang J (1998) Infrared radiation features of coal and rocks under loading. *Int J Rock Mech Min Sci* 35(7):969–976. [https://doi.org/10.1016/S0148-9062\(98\)00007-2](https://doi.org/10.1016/S0148-9062(98)00007-2)
- X-J. Liu, Z-B. Cheng, (2019) Changes in subsidence-field surface movement in shallow-seam coal mining. *Journal of the Southern African Institute of Mining and Metallurgy* 119 (2). <https://doi.org/10.17159/2411-9717/2019/v119n2a12>
- Xinjie L, Cheng Z, Jin D (2019) Performance Analysis of Soft Roadway Surrounding Rock in Yushujing Coal Mine. *Geotechnical and Geological Engineering* 1–9. <https://doi.org/10.1007/s10706-019-01040-7>
- Xue D, Zhou H, Liu J, Yi H (2012) Numerical simulation of stress wave propagation in coal-rock combination media. *Adv Mater Res* 594–597:542–551. <https://doi.org/10.4028/www.scientific.net/AMR.594-597.542>
- Yang S, Li Z, Wei W, Zhang J (2017) Influence of loose top-coal on support and surrounding rock relationship in longwall top-coal caving mining. *J China Coal Soc* 42(10):2511–2517. <https://doi.org/10.13225/j.cnki.jccs.2017.1008>
- Zhang Y, Cheng Z, Lv H (2019) Study on failure and subsidence law of frozen soil layer in coal mine influenced by physical conditions. *Geomechanics and Engineering* 18(1):97–109. <https://doi.org/10.12989/gae.2019.18.1.097>
- Zhang Z, Liu J, Wang L, Yang H, Zuo J (2012) Effects of combination mode on mechanical properties and failure characteristics of the coal rock combinations. *J China Coal Soc* 37(10):1677–1681
- Zhao Y, Jiang Y, Zhu J, Sun G (2008) Experimental study on precursory information of deformations of coal-rock composite samples before failure. *Chin J Rock Mech Eng* 27(2):339–346
- Zhao Z, Wang W, Dai C, Yan J (2014) Failure characteristics of three-body model composed of rock and coal with different strength and stiffness. *Trans Nonferrous Metals Soc China* 24(5):1538–1546. [https://doi.org/10.1016/S1003-6326\(14\)63223-4](https://doi.org/10.1016/S1003-6326(14)63223-4)
- Zhao Z, Wang W, Wang L, Dai C (2015) Compression-shear strength criterion of coal-rock combination model considering interface effect. *Tunn Undergr Space Technol* 47:193–199. <https://doi.org/10.1016/j.tust.2015.01.007>